1-1-2003

Capacitance-voltage techniques used to determine defect densities in amorphous germanium and microcrystalline-silicon

Joshua Peter Koch
Iowa State University

Capacitance-voltage techniques used to determine defect densities in amorphous germanium and microcrystalline-silicon

by

Joshua Peter Koch

A thesis submitted to the graduate faculty
in partial fulfillment of the requirements for the degree of
MASTER OF SCIENCE

Major: Electrical Engineering

Program of Study Committee:
Vikram L. Dalal (Major Professor)
Gary Tuttle
Joseph Shinar

Iowa State University
Ames, Iowa
2003

Graduate College
Iowa State University

This is to certify that the master's thesis of

Joshua Peter Koch

has met the thesis requirements of Iowa State University

Signatures have been redacted for privacy

TABLE OF CONTENTS

ABSTRACT

Hydrogenated Amorphous germanium and microcrystalline silicon are two potential materials for solar energy conversion. These materials usually have many deep trap levels in the gap arising from the nature of their growth. For this research, a capacitance-voltage technique using variable frequency and temperature to determine the density and energy levels of these deep defects is used.

Capacitance-voltage (C-V) measurements yield a wealth of information about a material. Electrical properties such as background doping concentration and built-in voltage are determined from this elementary technique. Many different methods in literature exist in determining trap concentration and energy. By utilizing frequency and temperature methods with simple C-V measurements the defect concentrations are obtained without the need for expensive equipment.

It is determined both material systems contain continuous distribution of defects continuous rather than discrete. The relationship of these defects with photovoltaic properties in these materials are also discussed

CHAPTER 1: DOPING PROFILE DETERMINATION

1.1 Introduction

Basic material properties may be obtained through use of capacitance-voltage (C-V) measurements. C-V measurements are an easy and quick means of obtaining several properties at low expense. Typically, different capacitance measurements are taken at a variety of applied bias (usually reverse) voltages. The capacitance measurements obtained by applying a small ac voltage of less than one volt at a frequency anywhere from 100 Hz to 10MHz to the sample and measuring the current.

1.2 Junction Capacitance Analysis

It has been shown doping densities within $p+n$ junction diodes may be derived from capacitance-voltage measurements. [1,2] C-V measurements determine the movement of charge within a semiconductor. Following is the result derived using Poisson's equation:

$$C = \left| \frac{d}{dV_j} qAN_D(x) \left(\frac{2\varepsilon_s V_j}{qN_D(x)\left(1+\frac{N_D(x)}{N_A(x)}\right)} \right)^{1/2} \right|$$

$$C = \left| A \sqrt{\frac{2\varepsilon_s qN_D(x)}{\left(1+\frac{N_D(x)}{N_A(x)}\right)}} \cdot \frac{1}{2\sqrt{V_j}} \right|$$

$$C = A \sqrt{\frac{\varepsilon_s qN_D(x)N_A(x)}{2(N_A(x)+N_D(x))V_j}} \qquad (1.1)$$

The easiest way to find the doping concentration is by plotting $1/C^2$ versus applied bias V_{bias} and finding the slope. See figure 1.1 for an example of C versus V_{bias} and $1/C^2$ versus V_{bias}.

N_A and N_D are represented as a function of depth x. The doping acceptor and donor concentrations are not always constant throughout. As the bias voltage increases, the depletion width increases. Samples are grown vertically; therefore any change in ion

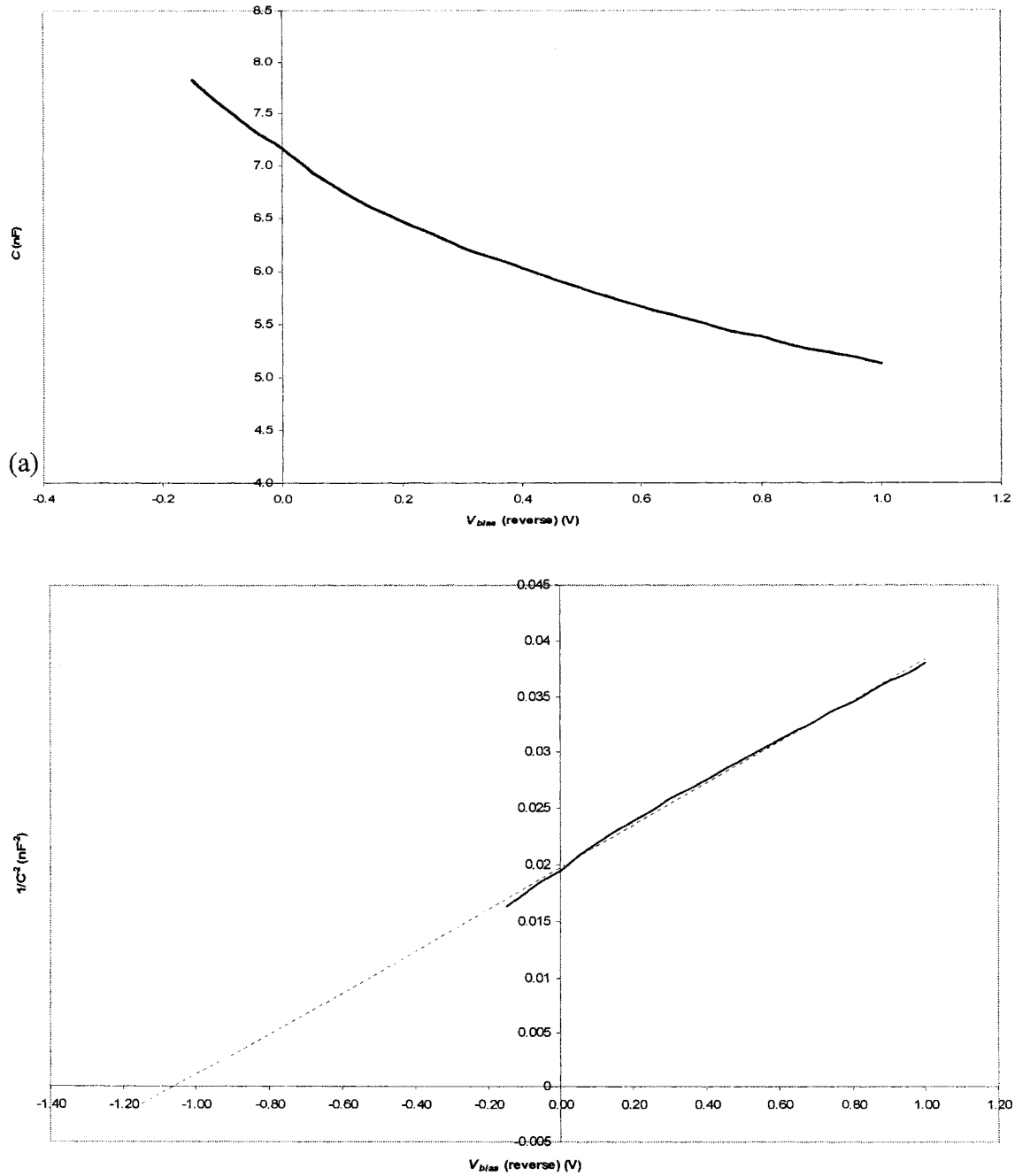

Figure 1.1. (a) A graph of junction capacitance versus applied reverse bias. Units for this C-V graph are nF for capacitance and V for the bias. (b) The data from the C-V graph rearranged in the $1/C^2$ versus V_{bias} form. The linearity shows a constant doping concentration. Also included is a linear trend line used to determine the built-in potential.

concentration, intentional or not, is a function of depth. Evidence of any non-linear doping is evident by plotting $1/C^2$ versus bias voltage. Instead of a linear plot (distinct doping concentrations), it may have separate slopes or be curved (graded doping concentrations).

1.3 Built-In Potential

The built-in potential, V_{bi}, of a junction is the barrier height (see figure 1.2a). Another way of viewing it is as the required potential to equalize the conduction bands.

$$V_j = V_{bi} \pm V_{bias} \tag{1.2}$$

Solving equation 1.20 for V_j yields a useful relation.

$$V_j = \frac{A^2}{C^2} \cdot \frac{q\varepsilon_s N_D(x) N_A(x)}{2(N_A(x) + N_D(x))} = V_{bi} \pm V_{bias} \tag{1.3}$$

The built-in voltage can be obtained either by determining the x-intercept of the $1/C^2$ versus V_{bias} graph or by equation 1.3. See figure 1.1(b) for an example of the first method.

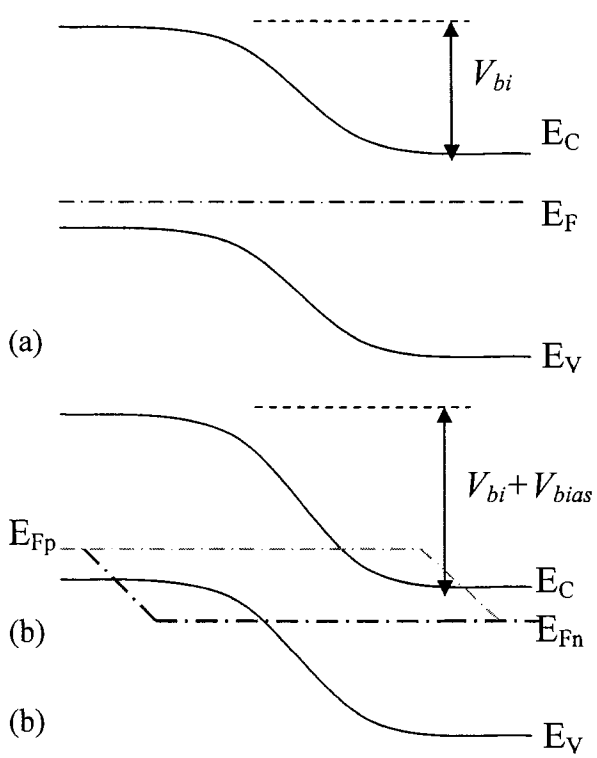

Figure 1.2. Energy band diagrams of the p+n junction shown (a) with and (b) without an applied bias. The bias shown here is a reverse bias of magnitude V_{bias}. With an added bias, the Fermi level splits and the barrier increases by V_{bias}.

CHAPTER 2: CHARACTERIZING DEFECT DENSITIES

2.1 Defect Creation

Defect densities in amorphous and microcrystalline materials arise from the processing technique used to create the sample and the properties intrinsic to the materials' nature. Processing, in general, yields the greatest contribution towards defect densities. Basic parameters, e.g. pressure and temperature, determine the type of material created. Subsequent parameters such as the gasses present in the plasma play an equally important role in determining the overall properties of the sample. By introducing hydrogen or helium gas to the plasma, dangling bonds within the sample are passivated thus reducing recombination centers. These recombination centers play a great role with the overall performance of the sample. Amorphous materials, or materials containing amorphous tissue, e.g. microcrystalline, contain a variety of states within the "forbidden gap" between the conduction and valence bands. The greatest of these are the recombination centers.

2.2 Trap Level Theory

The technique following assumes the sample consists of a p+n step junction.

To begin this discussion, assume the following band diagram for the p+n structure. Please note the system in figure 2.1 has no external bias applied. One distinct trap level is assumed in this derivation. Multiple discrete trap levels may exist and are determined according to superposition of the following technique. Multiple discrete and continuous trap levels are discussed following the single discrete case.

Detection of the trap depends on the location of the trap; the position of the trap level with respect to the Fermi energy determines the means with which to go about detecting and analyzing the trap. Traps that reside above the Fermi energy or close to the conduction band are easily detected by decreasing the drive frequency. Other deep traps, those at or below the Fermi energy, require a more aggressive approach. Temperature of

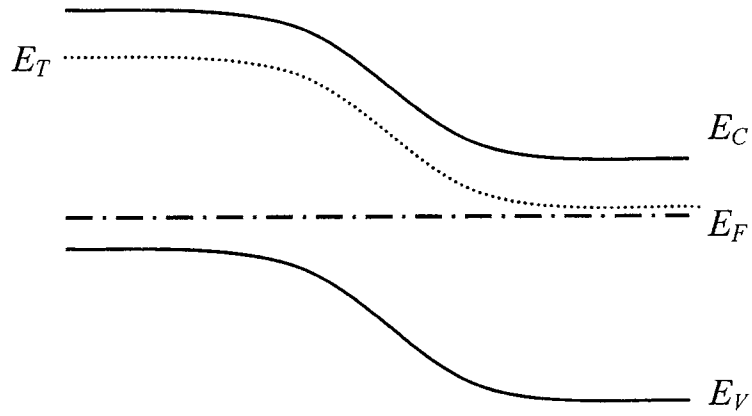

Figure 2.1. The band diagram of a p+n junction diode is shown here with one discrete shallow trap level. E_C is the conduction band edge energy position, E_V is the valence band edge energy position and E_T is the trap level.

the sample must then be increased to thermally stimulate the traps. Some traps may have energies low that a combination of lowering drive frequency and raising temperature are required. Several approaches are taken in literature to determine trap density and energy. Following are four most common methods used in literature.

2.2.1 Discrete Traps - Roberts and Crowell Technique

One of the first approaches to determining the effects of trap concentration was investigated by G. I. Roberts and C. R. Crowell in 1970. [3] Assuming a n-type semiconductor Schottky barrier with no negligible bias-dependent minority carrier density; the traps that contribute to the C-V measurement is then determined by the electrons only and their energy compared to the Fermi energy. An electron has a probability of being ionized given by Fermi-Dirac statistics as a function of the electrostatic potential.

$$f(\psi) = \frac{1}{g \cdot e^{-(q\psi - E)/kT} + 1} \tag{2.1}$$

Added to the ionization probability is a degeneracy factor, g. Assuming multiple discrete trap levels the charge distribution may be rewritten in terms of the ionization probability.

$$\rho(x)=\rho(\psi)=q\left[\left(\sum_D N_i f_i(\psi)-\sum_A N_i f_i(\psi)\right)-\left(\sum_D N_i f_i(\psi_f)-\sum_A N_i f_i(\psi_f)\right)e^{-q(\psi-\psi_f)/kT}\right] \tag{2.2}$$

This formula accounts for multiple donor and acceptor levels (D and A respectively) each of which has an independent ionization probability. Integrating equation 2.2 gives the total charge within the depletion region. This formula is quite length and those interested are directed to the Roberts and Crowell reference. Since both donor and acceptor trap levels are included in the derivation the formulas grow in length and complexity, however making a few assumptions based upon the material simplifies matters. A convenient parameter and normalization factor is defined if all of the donor levels ionize and acceptor contribution is minimized. This parameter, C_D, is then related to the Debye length L_D.

$$\frac{A\varepsilon_s}{C_D}=L_D=\sqrt{\frac{\varepsilon_s kT}{q^2\sum_D N_i}} \tag{2.3}$$

C_D is then used to normalize the capacitance measurements versus voltage plots. For large enough reverse bias voltages the normalized $(C_D/C)^2$ versus V curve assumes a linear form. However, at lower reverse bias voltages the traps become visible as bumps in the normalized plots. See figure 2.2 for a representation of this phenomena.

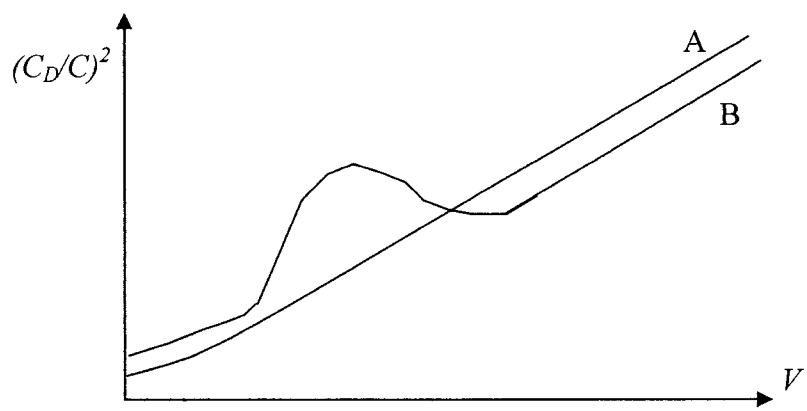

Figure 2.2. These are two different normalized C-V plots demonstrating the influence of shallow traps on the measurement. Curve A is one without any significant donor trap concentration. Curve B is shows one distinct trap level.

The approach by Roberts and Crowell is usefully in initially determining the presence of discrete donor traps. This method does not allow the determination of the existence of continuous traps or the energies associated with any discovered traps. Therefore other techniques must be utilized.

2.2.2 Discrete Traps – Cohen, et al., Technique

Another approach to determining trap characteristics, discussed by Cohen, et al.., utilizes adjustment of the drive frequency and temperature. [4] Detection of the trap depends on the location of the trap; the position of the trap level with respect to the Fermi energy determines the means with which to go about detecting and analyzing the trap. Traps that reside above the Fermi energy or close to the conduction band are easily detected by decreasing the drive frequency. Other deep traps, those at or below the Fermi energy, require a more aggressive approach. Temperature of the sample must then be increased to thermally stimulate the traps. Some traps may have low energies that a combination of lowering drive frequency and raising temperature are required. First, shallow traps are examined using the frequency approach. Second, inspection of deep traps through temperature variation is discussed. Third, a combination of the two approaches is investigated.

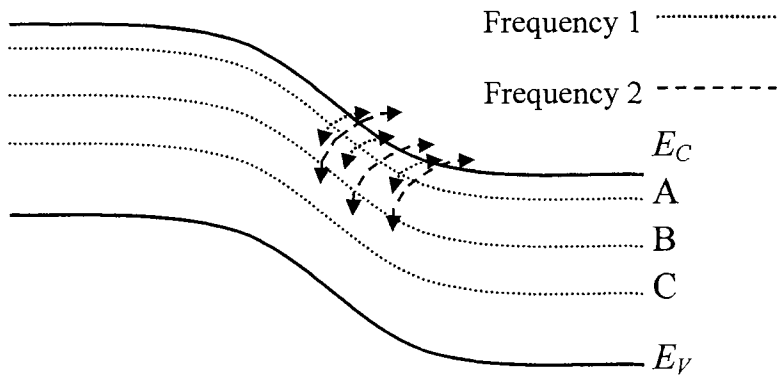

Figure 2.3. Influence of drive frequency on capacitance measurements. Shown are the conduction band edge (EC), valence band edge (EV), three different electron levels (A,B,C) and the filling and releasing of electrons for two different drive frequencies. Note frequency 1 is less than frequency 2.

2.2.2.1 Shallow Trap Detection

By lowering the drive frequency, electrons have a longer time in which to fill states below the conduction band edge. See figure 2.3 for a representation of this process. This figure also demonstrates the importance of the drive frequency on the capacitance measured. Note for drive frequency 1 the only electrons that contribute to the capacitance reading are those which have a time constant equal to or greater than the drive frequency, i.e. A on the figure and not B. The time constant for an electron is related to the inverse of the electron emission coefficient. [5]

$$\tau = \left(\sigma v_{th} N_c\right)^{-1} e^{(Ec_c - E_T)/kT} = \frac{1}{e_n(T)} \tag{2.4}$$

$$e_n(T) = \sigma v_{th} N_C e^{-(E_C - E_T)/kT} \tag{2.5}$$

$e_n(T)$ is the electron emission coefficient, σ is the capture cross section, N_c is the effective density of states at the conduction band and v_{th} is the thermal velocity. Note the high temperature dependence of the electron emission coefficient. Not only does it have an $e^{-1/T}$ dependence, but the electron capture cross section and thermal velocities depend on

temperature as well. For the discussion over frequency dependence, however, assume room temperature. Under this assumption equation 2.5 simplifies.

$$\nu_e = \nu_0 e^{-\left(E_C - E_T / kT\right)} \tag{2.6}$$

The quantity v_o is called the attempt-to-escape frequency and is around $10^{12} - 10^{13}\ s^{-3}$. [6] For discrete frequency steps the capacitance is not expected to change until the trap level is uncovered, i.e. the drive frequency $f < v_e$. The change in capacitance is then related to the trap density and energy. [7]

$$C = \frac{v_e^2}{v_e^2 + f^2} N_T A \sqrt{\frac{\varepsilon_s q}{2 N_D V_j}} \tag{2.7}$$

In the above equation f is the drive frequency.

2.2.2.2 Deep Trap Detection

For deep traps (those at or below the Fermi energy), decrease in frequency is not enough to uncover the traps. The assumption in the frequency approach was constant temperature so the electron emission coefficient should be rearranged for this case. [7]

$$e_n(T) = \sigma \gamma T^2 e^{-(E_C - E_T)/kT} \tag{2.8}$$

The constants have been grouped into the constant factor $\gamma = 16\pi K^2 m_e^* h^{-3}$. The electron emission coefficient is $T^2 e^{(-1/kT)}$ dependant. The dominating term is the T^2 term. Again, there is a point in which the increase of temperature allows the detection of deep traps.

2.2.2.3 Combined Approach

The final aspect desired from C-V measurements utilizing frequency and temperature dependence is obtaining the trap energy level. This approach may only be applied to discrete trap levels. Since both drive frequency and temperature vary the best way to obtain the trap energy from equation 2.5. [8]

$$f = e_n(T) = \sigma \gamma T^2 e^{-\left(E_C - E_T / kT\right)}$$

$$\ln\left(\frac{f}{T^2} \cdot \frac{1}{\sigma\gamma}\right) = -\frac{(E_C - E_T)}{kT} \tag{2.9}$$

$$\ln\left(\frac{f}{T^2}\right) = -\frac{(E_C - E_T)}{kT} - \ln(\sigma\gamma) \tag{2.10}$$

By plotting $\ln(f/T^2)$ versus $1/T$ one finds a line with slope to be that of the energy (divided by Boltzmann's constant) and the intercept relating to the capture cross section.

2.2.2.4 Multiple Discrete Traps

Most materials do not contain a single trap level, but rather several trap levels. To uncover these traps, a combination of drive frequency and temperature techniques may be required. Simply apply the principle of superposition to the technique, but keep in mind uncovered traps continue to contribute to capacitance measurements.

2.2.3 Continuous Trap Distributions - Glade, et al., Technique

Another approach which utilizes both of the above methods is one by Glade, Fuhs and Mell. [9] They suppose the capacitance measured as a function of frequency and temperature assume a slightly different form. The charge which contributes to conduction is broken into two different regions. See figure 2.4 for a representation of this division. The charge within the $x < x_w$ region behaves as a dielectric capacitor of capacitance $C_1 = \varepsilon_s / x_w$. The second region behaves as expected from Roberts and Crowell approach.

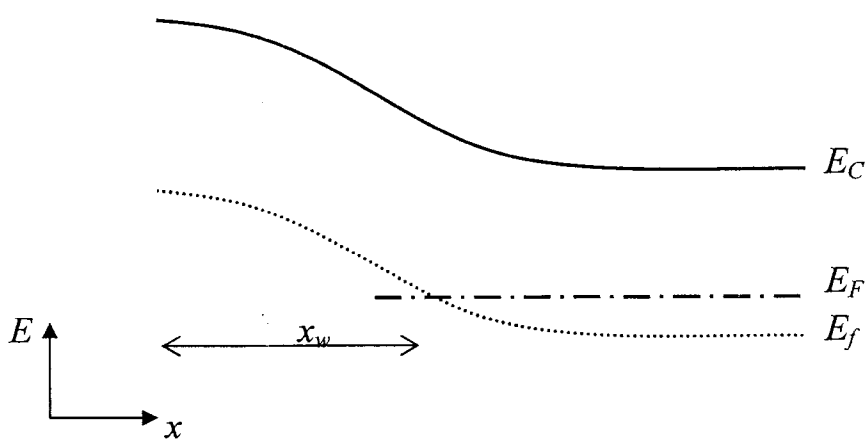

Figure 2.4. The Band diagram for a p+n junction depicting two regions: the "dielectric" space charge region ($x < x_f$) and transition region ($x \geq x_f$). The depth energy of the capacitance probe is also shown. Not shown is the valence band edge.

$$C_2 = \frac{\varepsilon_s \rho(E_F - E_f)}{\sqrt{\frac{2\varepsilon_s}{q}\int_0^{E_F - E_f} \rho(\psi) d\psi}} \tag{2.11}$$

In the above equation E_f is the depth of the capacitance probe. It is obtained by a relation between the drive frequency and temperature.

$$E_C - E_f = kT \ln\left(\frac{1}{2\pi f \cdot \tau_0}\right) \tag{2.12}$$

Again, τ_0 is the attempt-to-escape frequency and is assumed for this method to be $\sim 10^{-14}$ s. The resulting capacitance measurement is then a series of C_1 and C_2. The energy can then be extrapolated by use of equation 2.12.

2.2.4 Continuous Trap Distributions – Kimerling Method

Single trap levels are easily identified with the previous methods, but not as easily detected are continuous trap distributions. Such distributions are seen in amorphous materials or those containing amorphous tissue, e.g. microcrystalline materials. If traps are uniformly distributed, then steps in capacitance measurements are not present because such is only observed when discrete traps are uncovered. To understand continuous traps and how such are observed, a slightly varied approach is needed of the depletion region. [10]

Instead of a distinct space charge region and neutral region, a transition region between the two exists. This is similar to Glade, et al., except Kimerling assumes a neutral region beyond x. This transition region is of particular interest when dealing with deep traps. See figure 2.5. Traditionally when filling and empting trap levels, those above the Fermi alone (within width x in figure 2.5) were assumed to contribute to capacitance measurements. However, those electrons in traps beneath the Fermi energy may also become involved in filling and emptying. This assumption produces two distinct charge distributions: one within the space charge region and another within the transition region (figure 2.6).

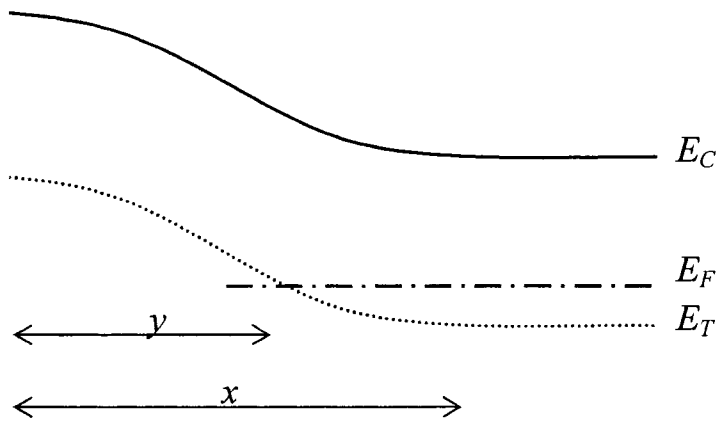

Figure 2.5. The Band diagram for a p+n junction depicting three regions: the space charge region (y), transition region (y-x) and neutral region. Although a single trap is shown, assume a continuous distribution of traps. Not shown is the valence band edge.

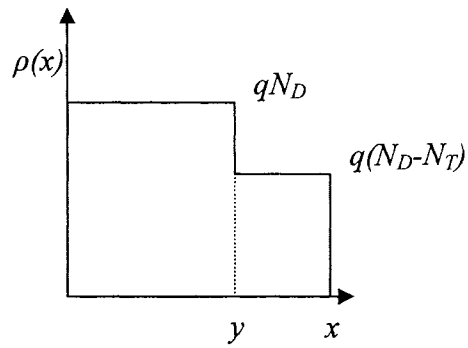

Figure 2.6. From figure 2.3, the corresponding charge distribution assuming the trap levels are acceptor levels.

To understand the physics behind the new depletion region, consider Gauss's Law. [11]

$$\int_{y}^{x} \vec{E} \cdot d\vec{l} = -V \tag{2.13}$$

$$\Delta E = \frac{\Delta V}{x} \tag{2.14}$$

The potential in equation 2.13 and 2.14 is related to the doping and width. [12]

$$\frac{\Delta V}{x} = \frac{q}{\varepsilon_s} N(x)\Delta x \tag{2.15}$$

Subsequent integration of equation 2.13 with the above substitution produces a relation to the energy, doping and transition region width.

$$\frac{1}{2}(x-y)^2 = \frac{\varepsilon_s}{q}\frac{(E_F - E_T)}{N(x)} \tag{2.16}$$

N(x) is the ion concentration determined from the C-V experiment which is a sum of the background doping concentration scaled by the trap concentration. The change in total charge uncovered relates to the ion concentration (see figure 2.4).

$$\Delta Q = \Delta Q(y) + \Delta Q(x) \tag{2.17}$$

$$\Delta Q(y) = qN_T(y)\Delta y \tag{2.18}$$

$$\Delta Q(x) = q(N_D(x) - N_T(x))\Delta x \tag{2.19}$$

$$\Delta Q = q(N_T(y)\Delta y + N_D(x)\Delta x - N_T(x)\Delta x) \tag{2.20}$$

Recall from chapter 1 the relation of capacitance to total depletion width W_D.

$$C = \frac{\Delta Q}{\Delta V} = \frac{\varepsilon_s}{W_D}$$

Combining equations 2.20 and 2.15 to find the total ion concentration in terms of the background doping and trap concentrations.

$$\frac{\Delta V}{x} = \frac{\Delta Q}{xC} = \frac{q}{\varepsilon_s}\frac{(N_T(y)y\Delta y + N_D(x)x\Delta x - N_T(x)x\Delta x)}{x} \tag{2.21}$$

$$\frac{\Delta V}{x} = \frac{q}{\varepsilon_s}\left(N_T(y)\frac{y\Delta y}{x\Delta x} + N_D(x) - N_T(x)\right)\Delta x \tag{2.22}$$

Equate equations 2.15 and 2.21.

$$N(x) = N_T(y)\frac{y\Delta y}{x\Delta x} + N_D(x) - N_T(x) \tag{2.23}$$

The assumption before was constant background doping concentration. For continuous distribution of traps and the background doping assumption, the total doping is constant. Therefore, in change in y is equal to the change in x, i.e. $\Delta y = \Delta x$. [13] In addition, deep traps between x and y do not contribute thus $N_T(y)$ may be replaced by $N_T(x)$.

$$N(x) = N_D(x) - N_T(x)\left(1 + \frac{y}{x}\right) = N_D(x) - N_T(x)\frac{x-y}{x} \tag{2.24}$$

Instead of obtaining constant doping concentration as a function of depth, the trap level is scaled by a factor of *(x-y)/x*. A representation of this relation is shown in figure 2.7.

For donor trap levels, a similar approach is used, but the trap concentration adds to the background level instead of being subtracted.

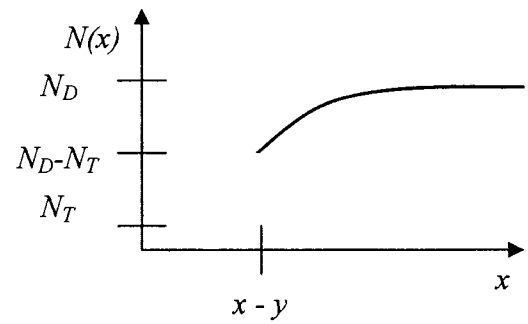

Figure 2.7. Total ion concentration obtained from C-V measurements with a continuous distribution of acceptor traps is not a constant value, rather a slope of *(x-y)/x* is noted beginning at *x-y*.

CHAPTER 3: EXPERIMENT

3.1 Description of Equipment

The C-V experiment for the amorphous germanium in this research utilizes the Stanford Research Systems SR 715 LCR meter. This meter contains four drive frequencies of 100 *Hz*, 120 *Hz*, 1 *kHz* and 10 *kHz*. Internal calibration, short and open, provides ease in use of this meter. The bias is provided externally. Additional nice features include three different sampling times and an average function to reduce noise. The one drawback of this meter is the inability to forward bias the sample beyond 0.2 *V*. An internal diode prevents any forward bias from being applied to the sample.

The 1 *MHz* frequency measurements are obtained using the HP 4275A LCR meter. This meter is quite similar to the SR 715, but its frequency measurement ranges from 10 *kHz* to 10 *MHz*.

The microcrystalline silicon samples are measured using the Agilent 4263B LCR meter. The meter has addition drive frequencies including the 100 *kHz* frequency used on the sample.

The external DC bias is provided by an Agilent E3610A DC Power Supply. Provided inside is current and voltage limited circuitry. The E3610A is an analog dial supply with a digital display. The digital display is the only limitation for the power supply due to its 0.1 *V* accuracy. Therefore, attached to the output of the power supply is a Keithley 177 Microvolt DMM. The accuracy of this meter is 0.001 *V*.

For temperature control a hot plate with AC voltage is used. However, the internal circuitry lead to leakage AC current within the plate that interfered with the LCR meter calibration and capacitance measurements. To compensate, the hot plate is wired with an external DC power supply provided by an HP Harrison 6443B DC Power Supply. This power supply is analog so a Keithly 169 Multimeter is attached to monitor the voltage.

To maintain the sample temperature, a small plate of aluminum is placed on the hot plate. Its purpose is to maintain the temperature once the hot plate is warmed to the appropriate temperature. If the temperature of the hot plate changes during the

measurement process then the aluminum plate dampens any change. Type-K thermocouples are attached to both the hot plate and aluminum plate and monitored by an Omega HH12 meter.

3.2 Description of Experimental Procedure

Experiments always begin by calibration of the LCR meters for that particular sample. In the case of the Aglient 4263B, the calibration occurs before measuring the sample for each drive frequency. The short calibration is performed upon the substrate and not by using a shorting wire. By using the substrate, any stray capacitance is compensated for during measurement. During this process the sample, hot plate and probes are covered to prevent any light from changing the measurement. The SRS LCR meter is set to C+R mode for parallel approximation, although placing it in series only makes a slight difference with the resistance measurement. [9] Once the calibration is complete all of the contacts are tested and the best contact is selected for the experiment. Acceptable contacts are those with 50 $k\Omega$ or larger for resistance at zero bias and frequencies under 10 *kHz*.

The experiment consists of the measuring the capacitance readings for all four frequencies of the SRS LCR meter for reverse bias voltages ranging from -0.15 V to 1.00 V. Temperature is then increased and the measurements taken again. Temperature readings are taken between room temperature and 100°C. Experiments in literature increase much greater than this, however high temperatures are not needed for this experiment. [10] Additional 10 *kHz* and 1 *MHz* frequency measurements are taken at room temperature using the HP LCR meter. The 10 *kHz* measurements provide a reference to the relative error of the two meters.

3.3 a-Ge:H and μc-Si:H Sample Information

The samples are produced by plasma enhanced chemical vapor deposition. They are grown on stainless steel substrates. Samples are *p-i-n+* diodes with ITO contacts deposited on top. Very small transition layers exist between the different regions, however their thickness is such that it can be ignored (~20-40*nm). The i-layer thicknesses of the samples range from 750μm* to 1000*μm*. Both a-Ge:H and μc-Si:H samples are pasivated with hydrogen.

CHAPTER 4: RESULTS AND DISCUSSION

4.1 a-Ge:H Results

The a-Ge:H sample is examined using the procedure described in chapter 3. Figures 4.1 and 4.2 show the C-V curve, $1/C^2$ versus V, respectively, used to determine the doping concentration and built-in voltage. The frequency used to for this graph is 1 kHz because, at room temperature, it should be such that no deep traps are uncovered thereby observing only the background doping concentration. Notice the $1/C^2$ versus V graph (figure 4.2) is linear. The linearity establishes the background doping concentration is constant. From equation 1.20 the background doping concentration is $7.55 \cdot 10^{16} \pm 0.38 \cdot 10^{16}$ $1/cm^3$. By continuing the graph down until it intercepts the x-axis, the built-in voltage is found to be 0.238 ± 0.022 V.

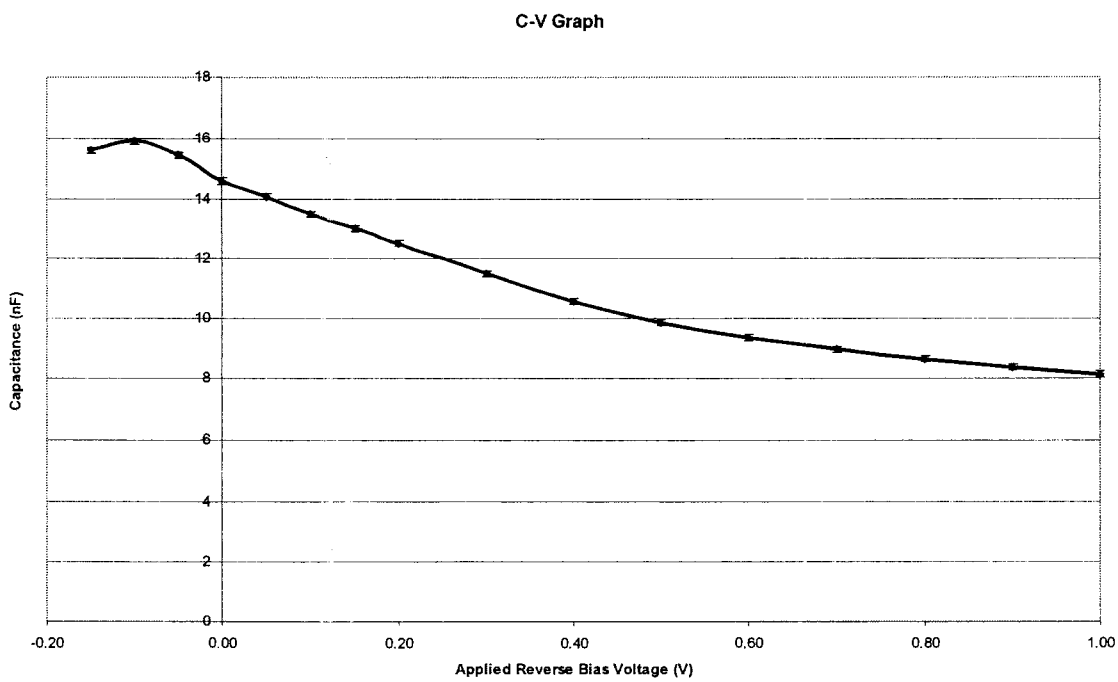

Figure 4.1. The graph of junction capacitance versus applied reverse bias for the amorphous germanium sample (2/6316). Units for this C-V graph are nF for capacitance and V for the bias.

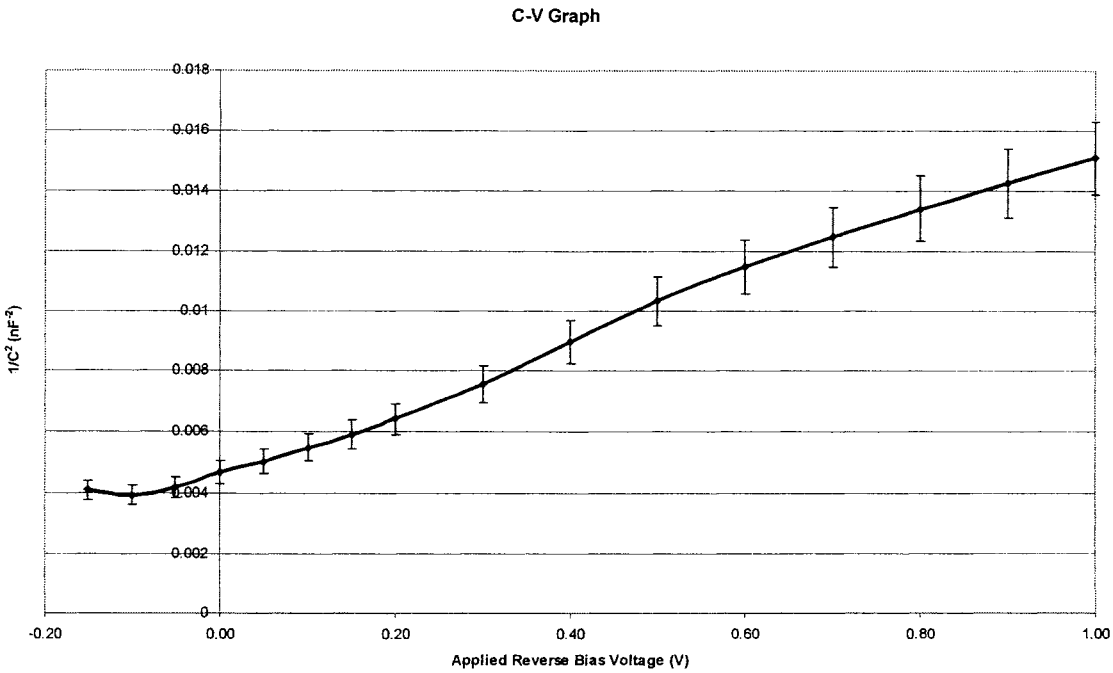

Figure 4.2. The data from the C-V graph in figure 4.1 is rearranged in the $1/C^2$ versus V_{bias} form. The linearity shows a constant doping concentration for the a-Ge:H sample (2/6316).

This data is consistent with those obtained in literature with other amorphous materials. [14]

Following are the results of the four methods described in chapter 2. Homogeneous trap distribution is expected for these cases however all four approaches are implemented.

4.1.1 Discrete Traps - Roberts and Crowell Technique

This approach requires that all donors be ionized therefore the assumption made is the total ionization occurs at the lowest frequency and highest temperature. Figure 4.3 shows the results of this analysis. As noted, no maxima occur on the graph and it looks as that of figure 4.2. Thus there is no discrete traps noted in this sample through this technique and the disadvantage of this technique is discovered.

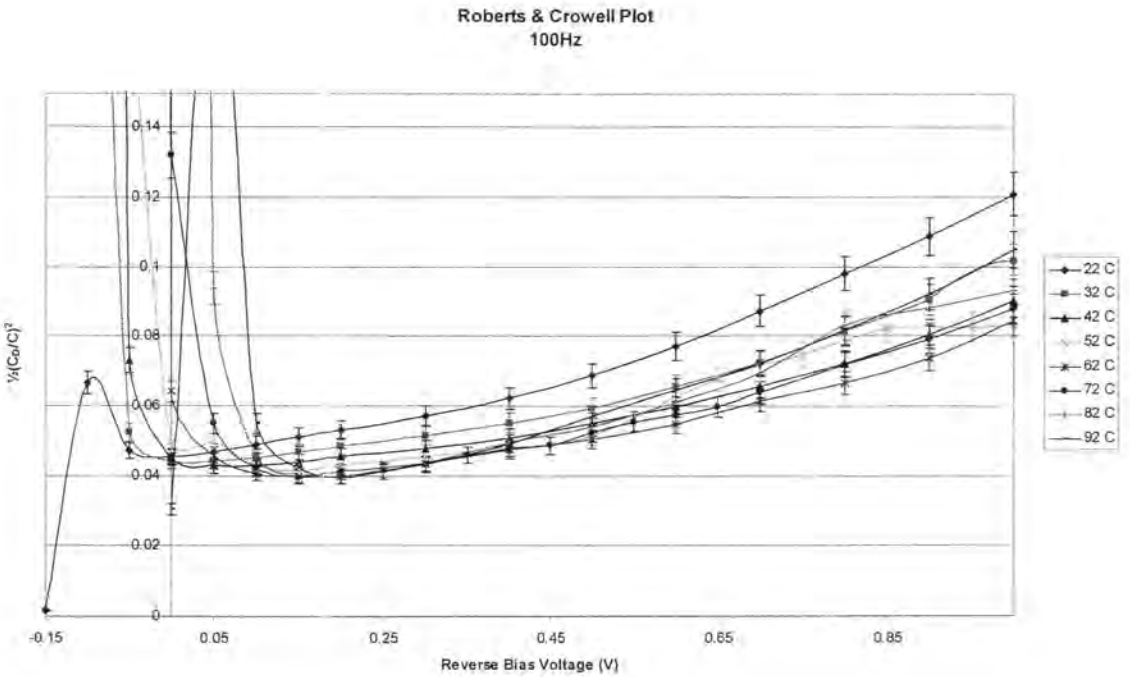

Figure 4.3. The data from the C-V graph in figure 4.1 is rearranged in the normalized $1/C^2$ versus V_{bias} form. The linearity shows a constant doping concentration for the a-Ge:H sample (2/6316).

4.1.2 Discrete Traps – Cohen, et al., Technique

Cohen and associates use two different methods separately and in parallel to determine the presence of and characteristics of traps. As mentioned in chapter 2, the drive frequency is decreased to determine the existence of shallow traps then the temperature is increased to find deep traps.

4.1.2.1 Shallow Trap Detection

Figure 4.4 shows the frequency dependence of the capacitance measurements. As expected, the capacitance decreases with increasing frequency. However, the decrease is uniform and not a step. This shows the trap distribution is continuous (for shallow depths) and not discrete. Shown in figure 4.3 are the cases with no bias and a slight reverse bias voltage. Notice how at 1 *kHz* and 10 *kHz* ranges the lines are approximately parallel. This also agrees with theory because it shows that traps are not being uncovered

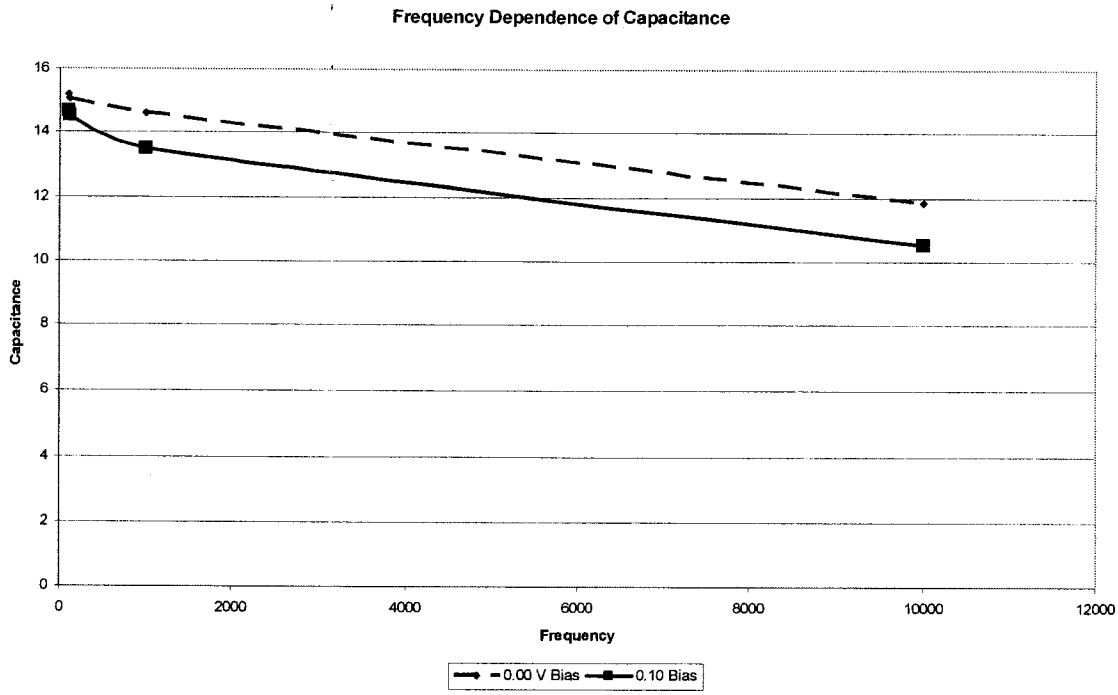

Figure 4.3. The a-Ge:H frequency dependence of capacitance curve for sample 2/6316

at those frequencies. If they were, the graph would not be linear in those regions. However, at the low frequencies of 100 Hz and 120 Hz there is evidence of uncovered traps. Since continuous the data indicates continuous trap distributions (theory as well) further methods are used to characterize them.

4.1.2.2 Deep Trap Detection

The frequency case showed the existence of shallow traps, however to unveil the whole trap distribution temperature is employed. The frequency used for this approach is 100 Hz. By using the lowest frequency the equipment allows, deeper depths may be examined. Figure 4.4 shows temperature variance for the sample. The data also indicates continuous trap distributions; therefore this method cannot be used to determine the trap concentration. The 1 *MHz* line is also plotted to show the case in which only the extremely shallow states are uncovered.

4.1.2.3 Combined Approach

The combined approach is not needed for this case. Both the temperature and frequency measurements indicated continuous trap distributions.

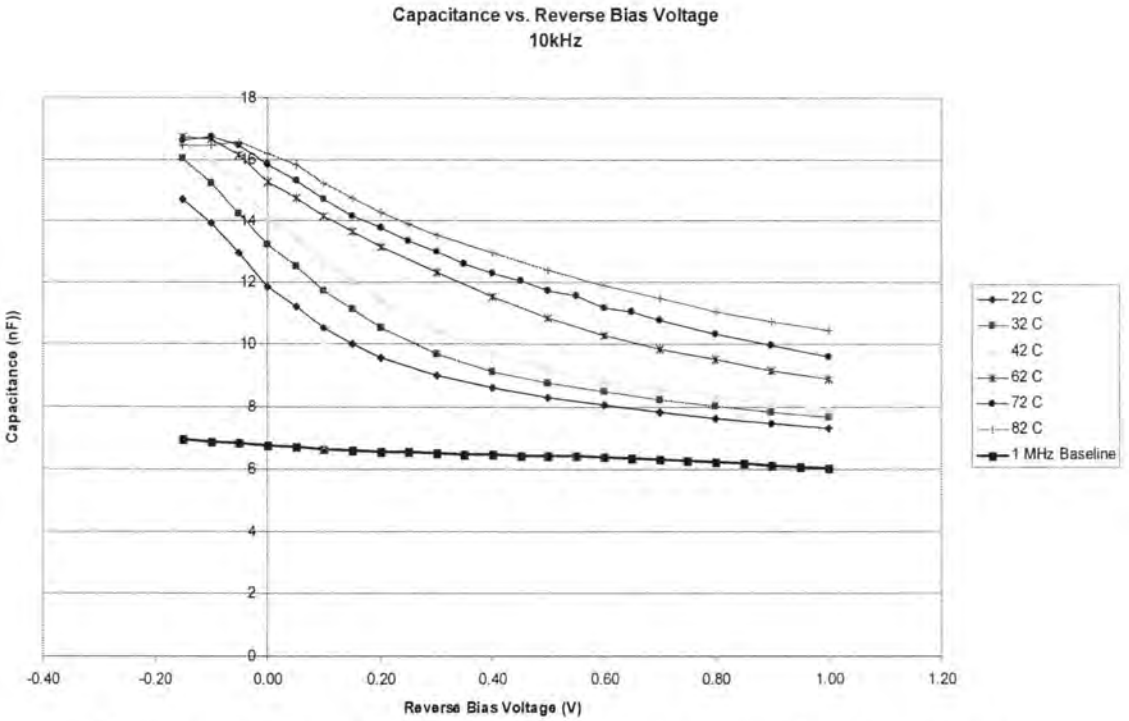

Figure 4.4. The a-Ge:H temperature dependence of capacitance for sample 2/6316

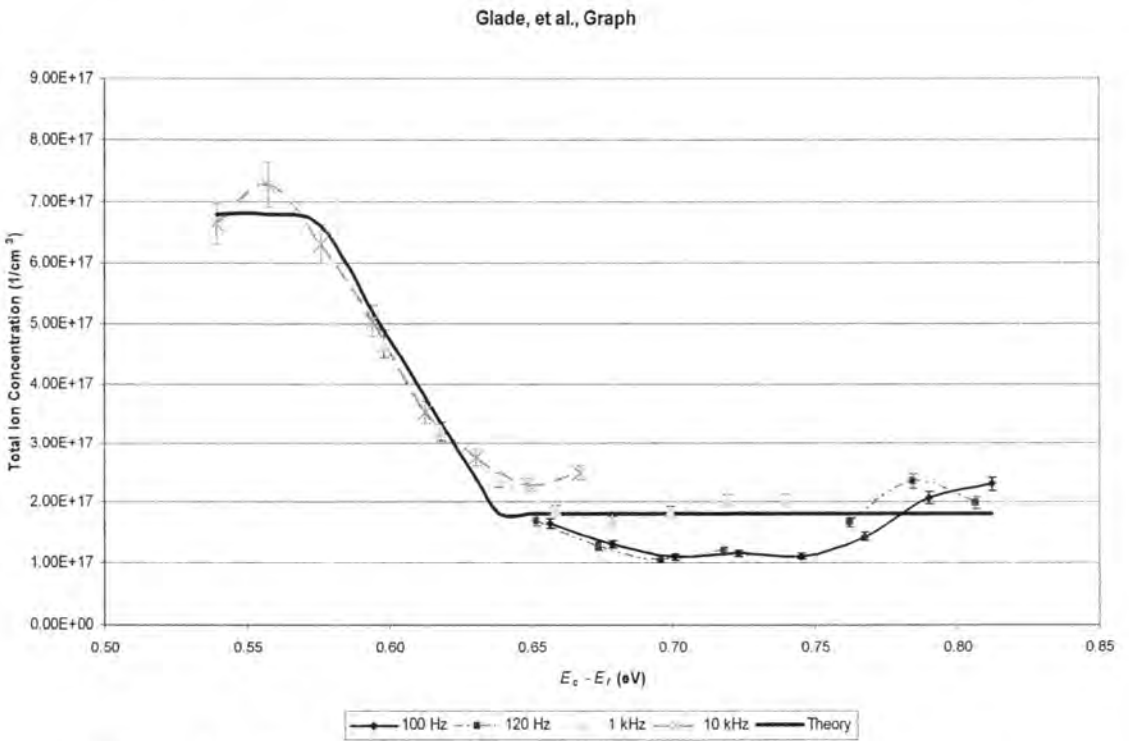

Figure 4.5. The Glade, Fuhs and Mell plot for four frequencies for the a-Ge:H sample (2/6316).

4.1.2.4 Multiple Discrete Traps

Since this sample contains continuous distribution of traps, this method is not applicable.

4.1.3 Continuous Trap Distributions - Glade, et al., Technique

This method takes quite a different approach to determining trap concentration and density. Although it is not as accurate as the final method, it provides a rough estimate. This method utilizes all of the data taken at all frequencies and temperatures. There is only one value of the defect density obtained from this method. Figure 4.5 shows the results of this analysis. For the higher frequency, the increase in depth (obtained through varied temperature) decreases the total ion concentration. The lower frequency shows a decrease in ion concentration and eventually, as with the 100 Hz measurement, it levels out to an almost constant value. This shows the presence of deep acceptor traps. The difference between the maximum value and minimum value yields the trap level. Note there is no significant cutoff energy at which the ion concentration drops off, rather a gradual slope. This indicates a continuous concentration of acceptors as was assumed before the measurements. The donor trap concentration is therefore determined to be $5.6 \cdot 10^{17} \pm 0.53 \cdot 10^{17}\ cm^{-3}$. This, however, does not agree with SCLC experiments and literature.

Plotted in figure 4.5 is also the theoretical plot from equations 2.11 and 2.12. The data and theory agree well. However, this density does not seem reasonable for this particular sample. The density expected from similar samples and literature for this sample is of the order of $10^{16}\ cm^{-3}$.

This measurement is sensitive to variations in temperature and frequency; increasing the frequency by a factor of ten yields a decrease in the difference between the conduction band edge and the Fermi level by 0.05 *eV*. Any slight variation in frequency caused by internal, equipment error, or external sources will skew the data. The greatest source of error in this measurement is temperature due to the equipment; an increase in temperature by 10°C increases the energy difference by 0.02 *eV*. Large amounts of time

are given to level the temperature gain between readings, but increases still occur. Thus this method is not the best for determining the defect density.

4.1.4 Continuous Trap Distributions – Kimerling Method

Figures 4.6-4.8 depict the data obtained from the experiment. This method obtains different values for each frequency and temperature. Included in figures 4.6-4.8 is the 1 MHz data used as a reference for when almost none of the donors or acceptors are ionized. As expected, it is approximately a horizontal line. This approach yields graphs comparable to those predicted by theory (equation 2.24 and figure 2.7). The amorphous nature of the material suggests continuous distribution of acceptor traps. The background doping concentration of $7.55 \cdot 10^{16} \pm 0.38 \cdot 10^{16}$ $1/cm^3$ helps to determine the type of traps present. The data shows levels under the background doping concentration which suggests acceptor trap levels. Using the theory previously derived for acceptor trap levels, the trap concentration is determined to be $3.32 \cdot 10^{16} \pm 0.17 \cdot 10^{16}$ $1/cm^3$. This is

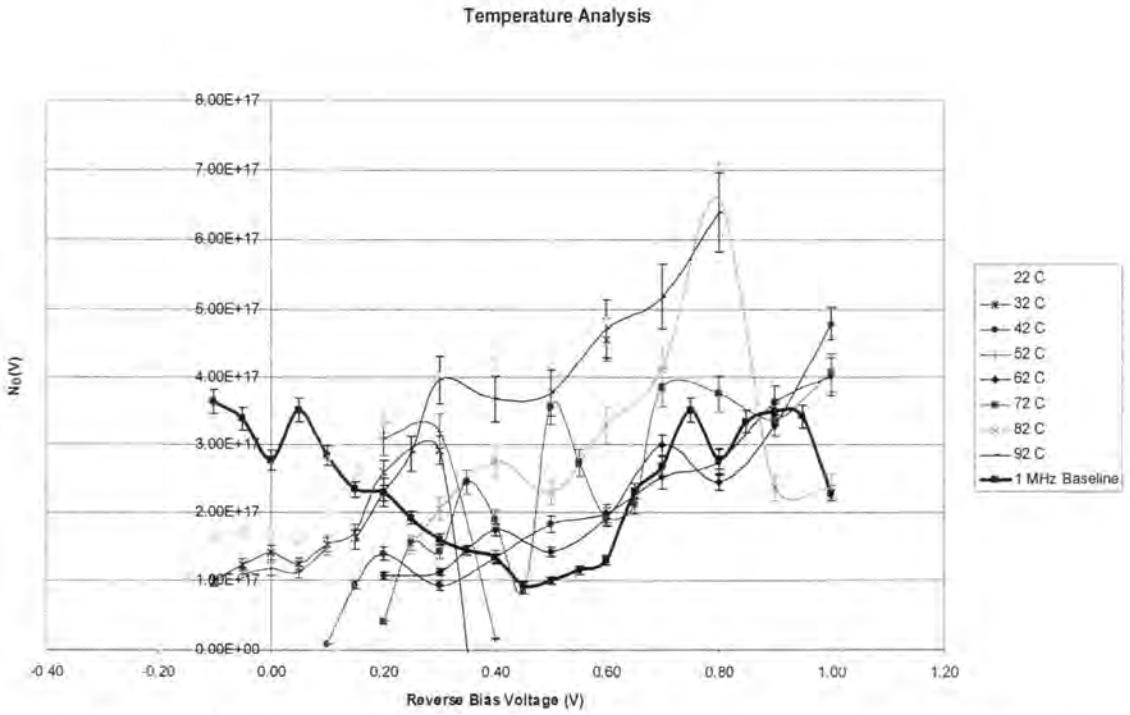

Figure 4.6. The total ion concentration for the a-Ge:H sample (2/6316) as a function of reverse bias voltage for the drive frequency of 100 Hz

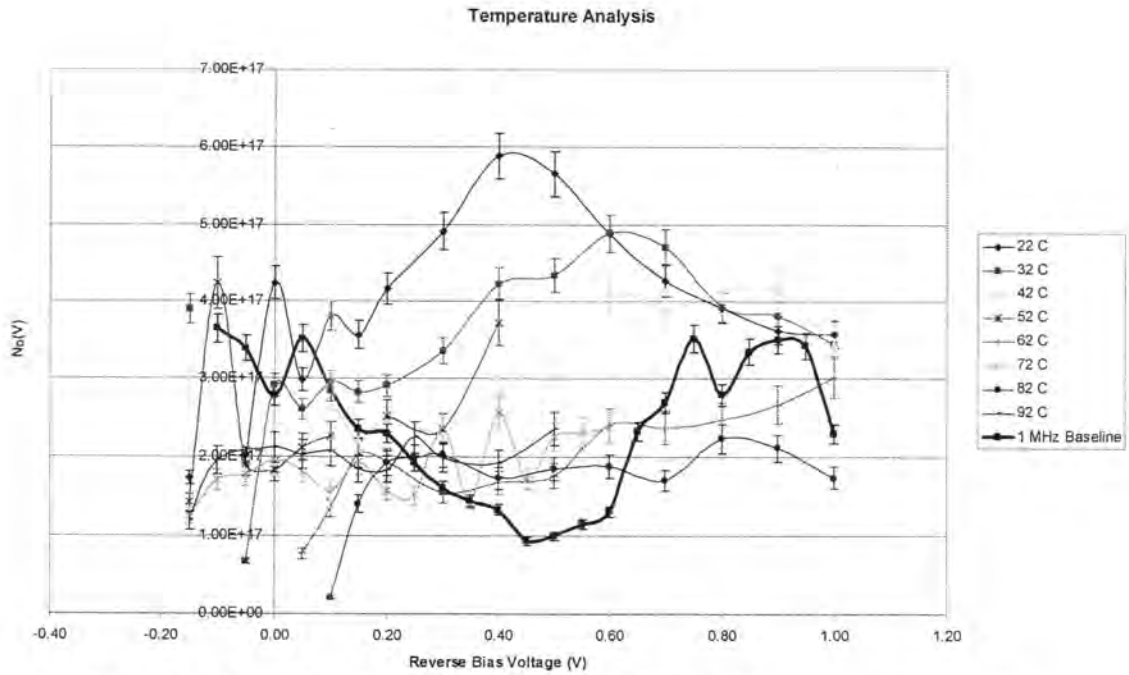

Figure 4.7. The total ion concentration for the a-Ge:H sample (2/6316) as a function of reverse bias voltage for the drive frequency of 1 kHz

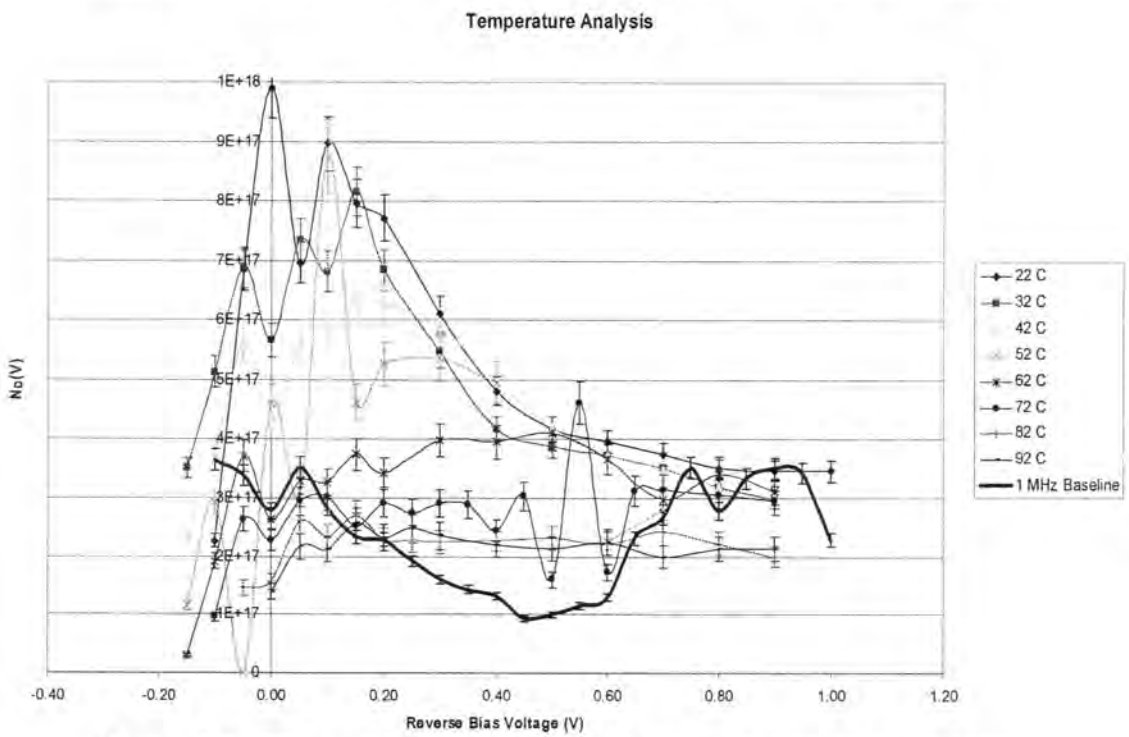

Figure 4.8. The total ion concentration for the a-Ge:H sample (2/6316) as a function of reverse bias voltage for the drive frequency of 10 kHz shows surface states at low reverse bias voltages for low temperatures.

obtained from the 100 Hz graph by taking the difference between the plateau of the graphs, also verified by the 1 MHz data, and the point at which the tail begins. This also agrees with previous measurements of defects within amorphous germanium from space charge limited current (SCLC) measurements of similar samples. [15]

One particular different observation is that of the 10 kHz case. Instead of usually decreasing for low reveres biases, it increases. This indicates a high concentration of ions for short depths. Vincent, et al., has also noted such concentrations. High concentrations of ions at short depths are attributed to surface states. These are noted for the high frequency case at low temperatures. See the low temperature cases for figure 4.6. The initial lower temperatures indicate the surface states, but when either the frequency or temperature is changed to increase the depth the surface the graph shows the theoretical graph for traps.

Thermal emission is important to discovering the profile of the sample. The sample contains acceptor traps so a decrease in the density function is expected as the temperature increases. This phenomenon takes place because more electrons are thermally stimulated to fill trap levels and thus the overall density decreases. Figures 4.6-4.8 all demonstrate this decrease in density as temperature increases. For example look at the results from the 100 Hz case, selected because a greater amount of traps are uncovered at this low frequency. Defect densities of $3.85 \cdot 10^{16} \pm 0.19 \cdot 10^{16}$ $1/cm^3$, $3.06 \cdot 10^{16} \pm 0.18 \cdot 10^{16}$ $1/cm^3$ and $2.22 \cdot 10^{16} \pm 0.13 \cdot 10^{16}$ $1/cm^3$ are derived from the temperatures 22°C, 42°C and 62°C respectively. By combining the temperature and frequency measurements a full picture of the sample's profile is revealed.

As noted before, the frequency has some effect in revealing traps at different levels. Evidence of this is seen in figure 4.9. Defect densities of $3.85 \cdot 10^{16} \pm 0.19 \cdot 10^{16}$ $1/cm^3$, $1.89 \cdot 10^{16} \pm 0.09 \cdot 10^{16}$ $1/cm^3$ and $1.24 \cdot 10^{16} \pm 0.06 \cdot 10^{16}$ $1/cm^3$ are observed from the 100 Hz, 1 kHz and 10 kHz data respectively. All of the different frequencies taper off to a common value which is also validated by the 1 MHz data. By increasing the drive frequency the probability of electron emission is less so a decrease in the density function is expected. Figure 4.9 demonstrates this exceptionally.

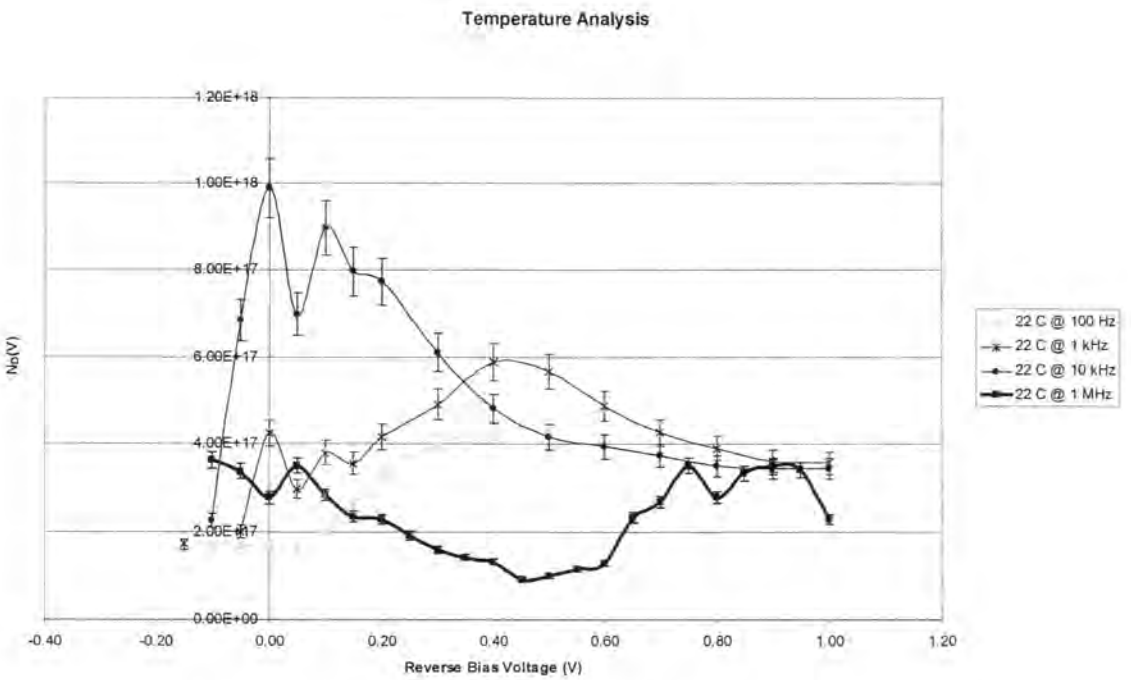

Figure 4.8. The total ion concentration for the a-Ge:H sample (2/6316) as a function of reverse bias voltage for a constant temperature and multiple drive frequencies show the frequency dependence of Kimerling's method.

Kimerling's method is not as sensitive to variations in frequency and temperature as the previous method. The graphs, with the exception of the 10 kHz case, agree with each other in derived defect densities.

This method is the preferred method because it agrees with both SCLC data and literature.

4.2 μc-Si:H Results

The same method of determining the background ion concentration and built-in voltage is employed as with the amorphous germanium sample. See figures 4.10 and 4.11. The microcrystalline-silicon sample has a background doping of $4.82 \cdot 10^{15} \pm 0.0735 \cdot 10^{15}$ $1/cm^3$ and a built-in voltage of 0.68 ± 0.034 V. The $1/C^2$ versus V curve is not linear in this case (see figure 4.11). This indicates graded doping with increasing concentration with depth .

The trap levels are expected to include continuous levels. However, discrete levels may exist within the crystallites. By utilizing both frequency and temperature approaches, the trap levels are examined.

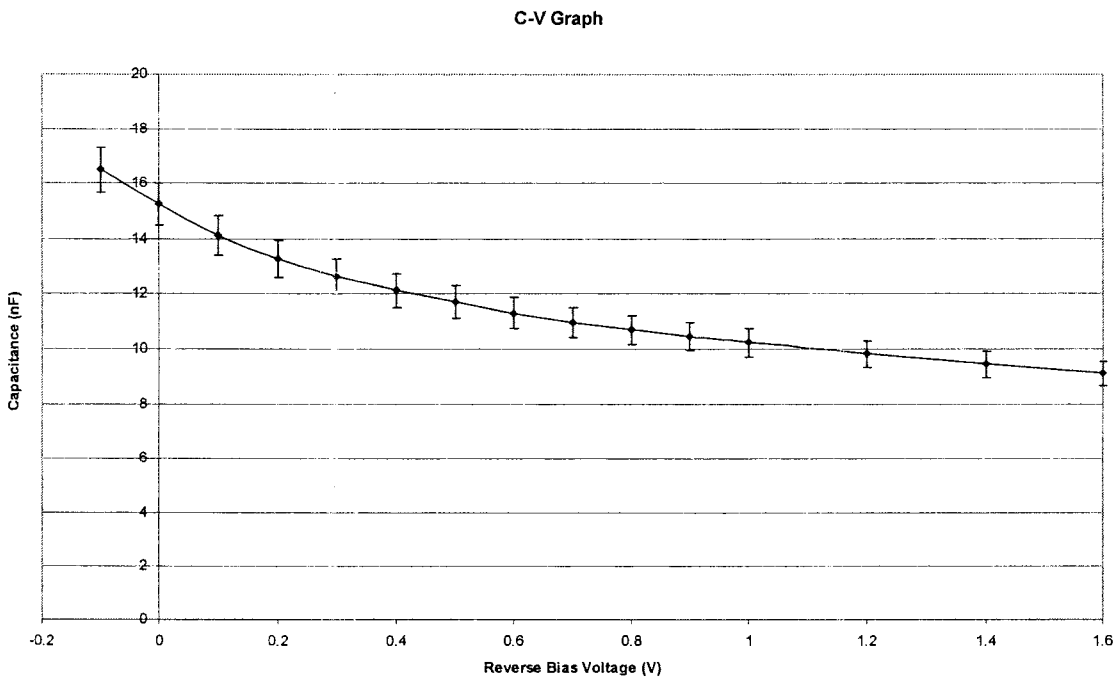

Figure 4.10. The graph of junction capacitance versus applied reverse bias for the μc-Si:H sample (2/6489).

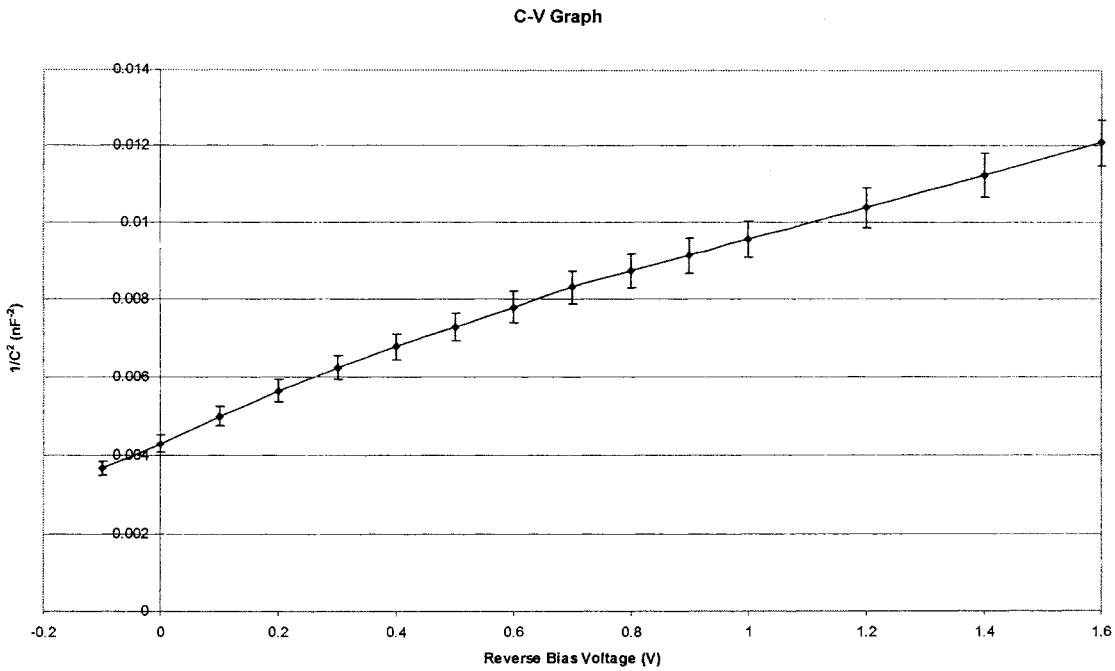

Figure 4.11. The data for the μc-Si:H sample (2/6489) from the C-V graph in figure 4.7 is rearranged in the $1/C^2$ versus V_{bias} form.

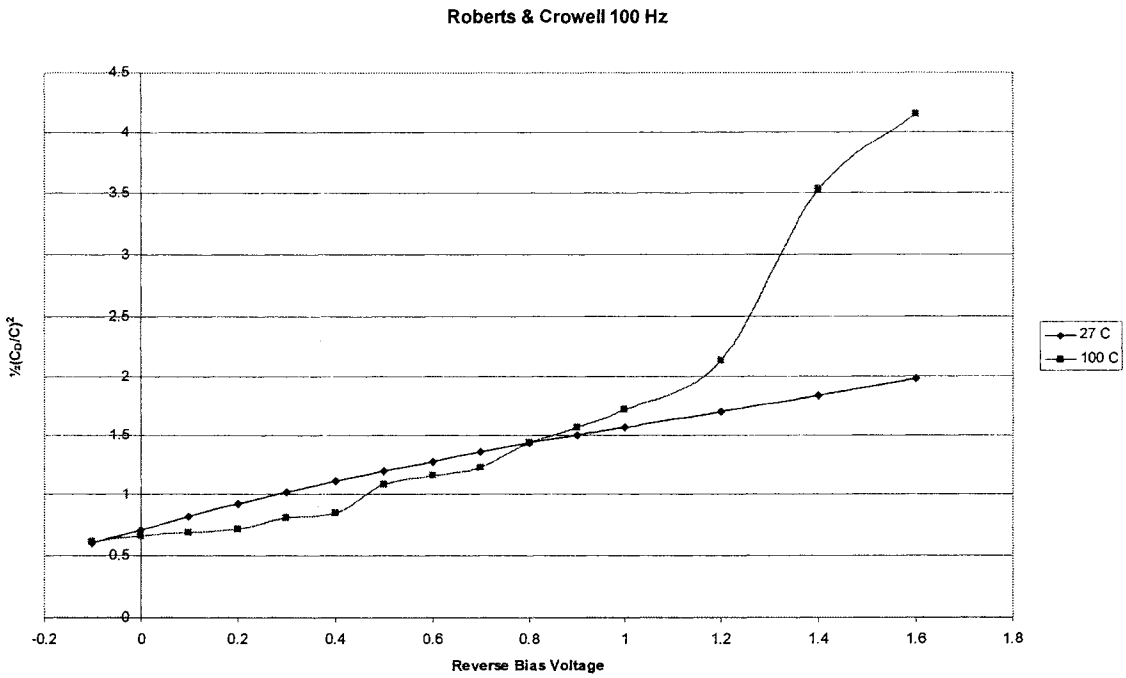

Figure 4.12. The normalized Roberts & Crowell plot for the μc-Si:H sample (2/6489).

4.2.1 Discrete Traps - Roberts and Crowell Technique

An initial investigation of the sample and its trap properties is performed. As seen in figure 4.12, there is no evidence of discrete traps within this sample.

4.2.2 Discrete Traps – Cohen, et al., Technique

Assuming continuous trap distributions from the Roberts and Crowell method these techniques do not yield much more information. However they are analyzed to possibly yield further information.

4.2.2.1 Shallow Trap Detection

Figure 4.13 shows the frequency dependence of the capacitance for the μc-Si:H sample. The capacitance decreases with increase in frequency, but the difference in between the two bias voltages is not the same as frequency increases to the high frequency case. This is expected because high drive frequencies should converge upon the geometric capacitance thus ignoring any deep states. However, a slight nonlinearity

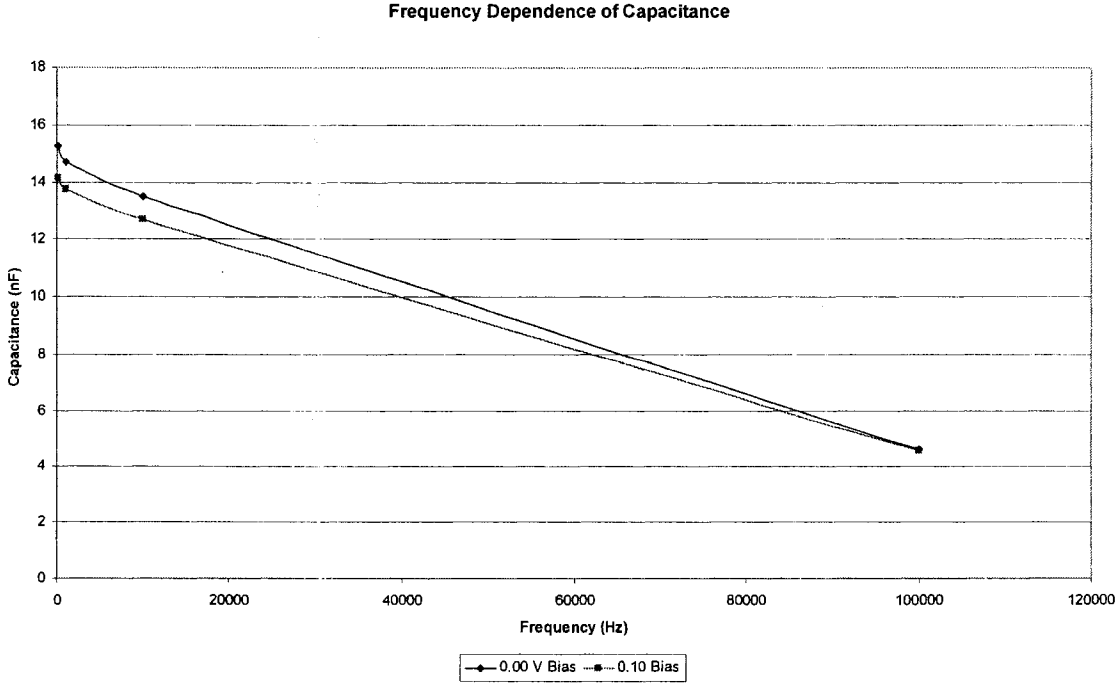

Figure 4.13. The frequency dependence of capacitance for the μc-Si:H sample (2/6489)

is noted for low drive frequencies showing the existence of deep.

4.2.2.2 Deep Trap Detection

Through temperature variation deep traps are uncovered. The data again suggests continuous trap distributions as in the amorphous germanium. Therefore no trap concentration is able to be obtained. Figure 4.14 shows the results of the change in temperature.

4.2.2.3 Combined Approach

The combined approach is not needed because no discrete trap levels are present.

4.2.2.4 Multiple Discrete Traps

No discrete traps were observed in this sample so multiple discrete traps cannot exist.

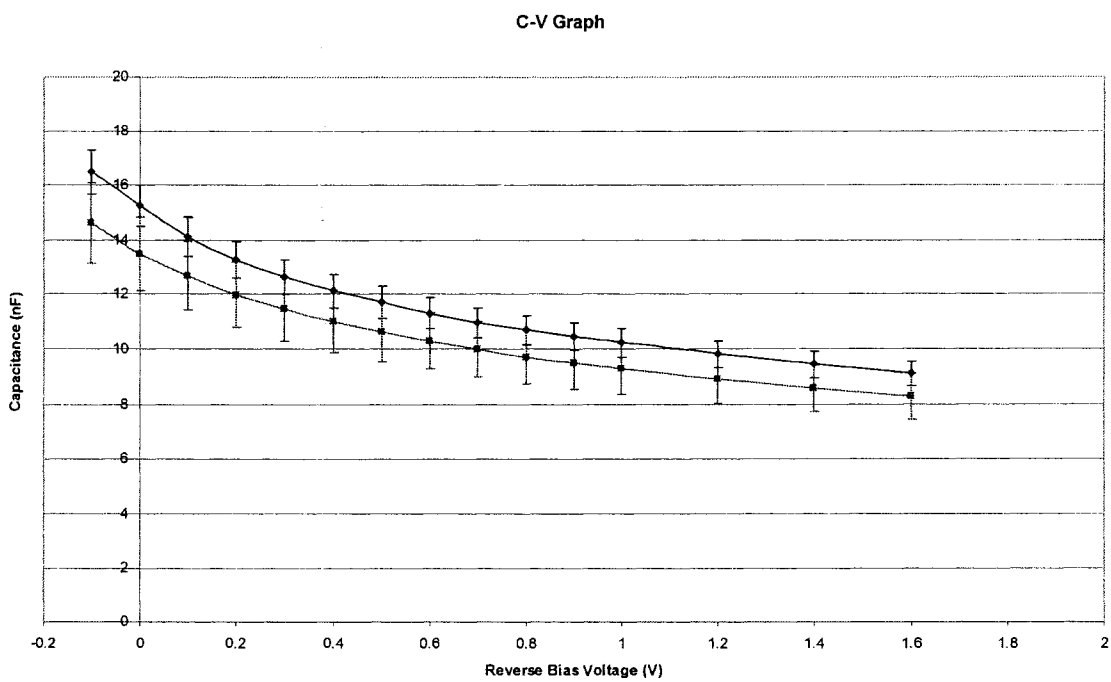

Figure 4.14. The total ion concentration for the μc-Si:H sample (2/6489) as a function of reverse bias voltage for the drive frequency of 100 Hz

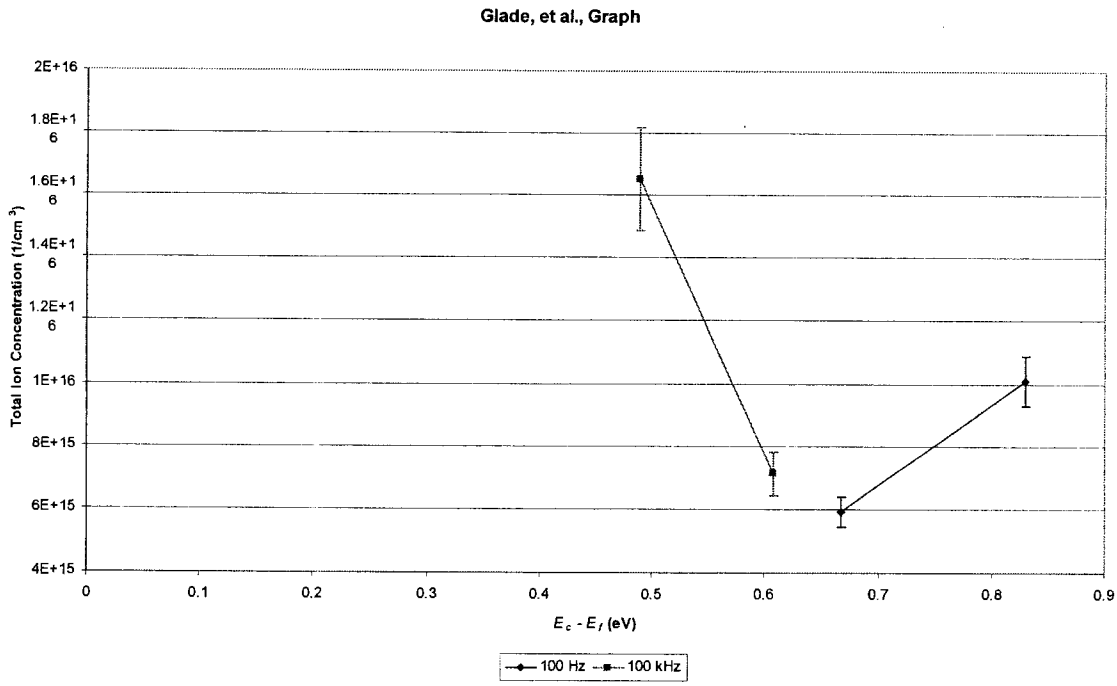

Figure 4.15. The Glade, Fuhs and Mell plot for two frequencies for the μc-Si:H sample (2/6489).

4.2.3 Continuous Trap Distributions - Glade, et al., Technique

The temperature measurements showed too much error in the readings therefore this method cannot be used. Although difficult to ascertain, it may be noted theory and data approximately could possibly match, however without further intense measurements no conclusions are drawn. Again, the details of this method as described for the a-Ge:H sample apply here as well.

4.2.4 Continuous Trap Distributions – Kimerling Method

Figures 4.16-4.19 graphs the results of this method. The temperature approach yielded trap concentrations which agree with amorphous materials. This was expected because of the amorphous tissue between the crystallites. Using the trap theory of Kimerling in chapter 2, the trap concentration is found to be $4.10 \cdot 10^{15} \pm 0.21 \cdot 10^{15}$ $1/cm^3$. This approach does not yield any proof of any discrete levels. Other experiments using SCLC on similar samples yielded similar results on the order of $\sim 10^{15}$ $1/cm^3$. [16]

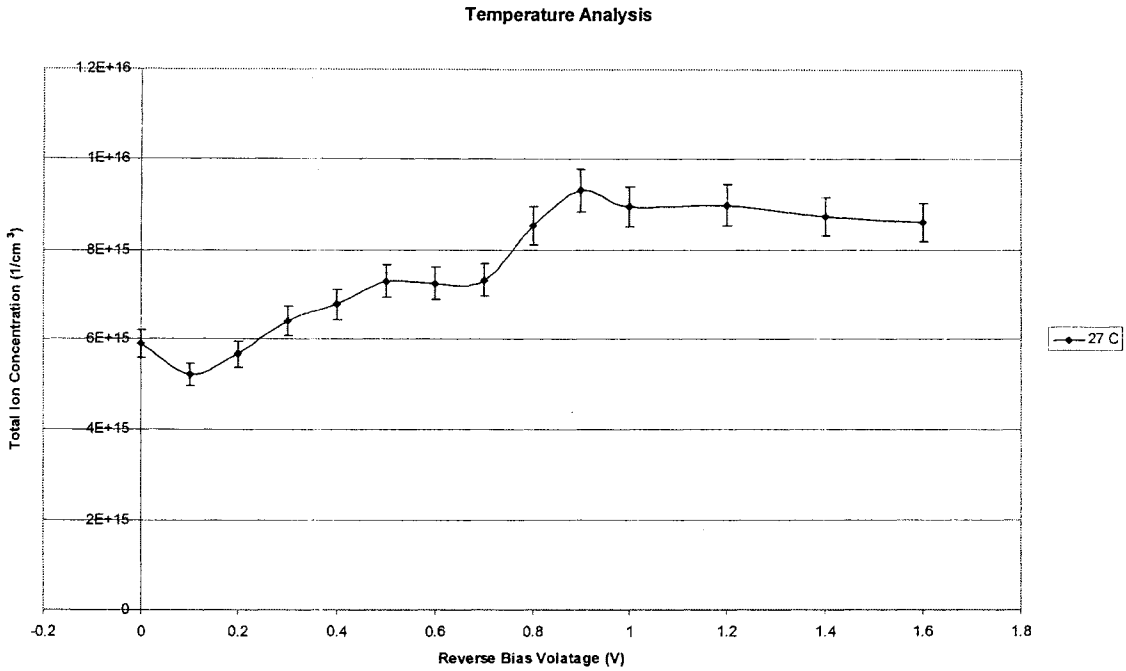

Figure 4.16. The total ion concentration for the μc-Si:H sample (2/6489) is shown as a function of reverse bias voltage for the drive frequency of 100 Hz.

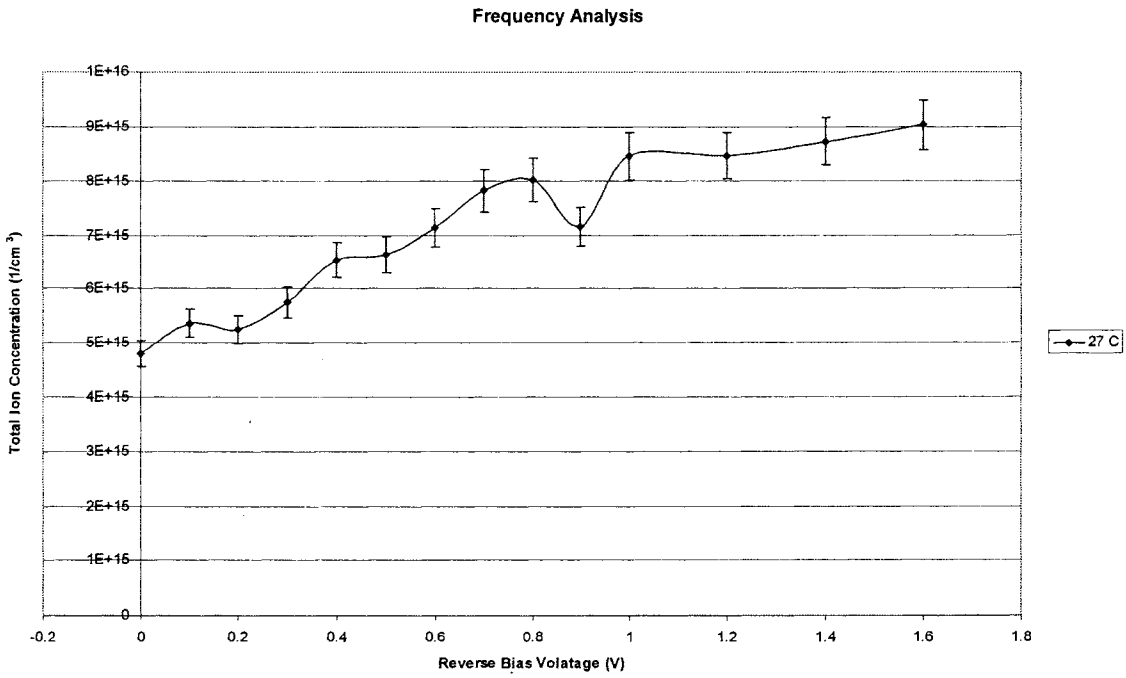

Figure 4.17. The total ion concentration for the μc-Si:H sample (2/6489) is shown as a function of reverse bias voltage for the drive frequency of 1 kHz.

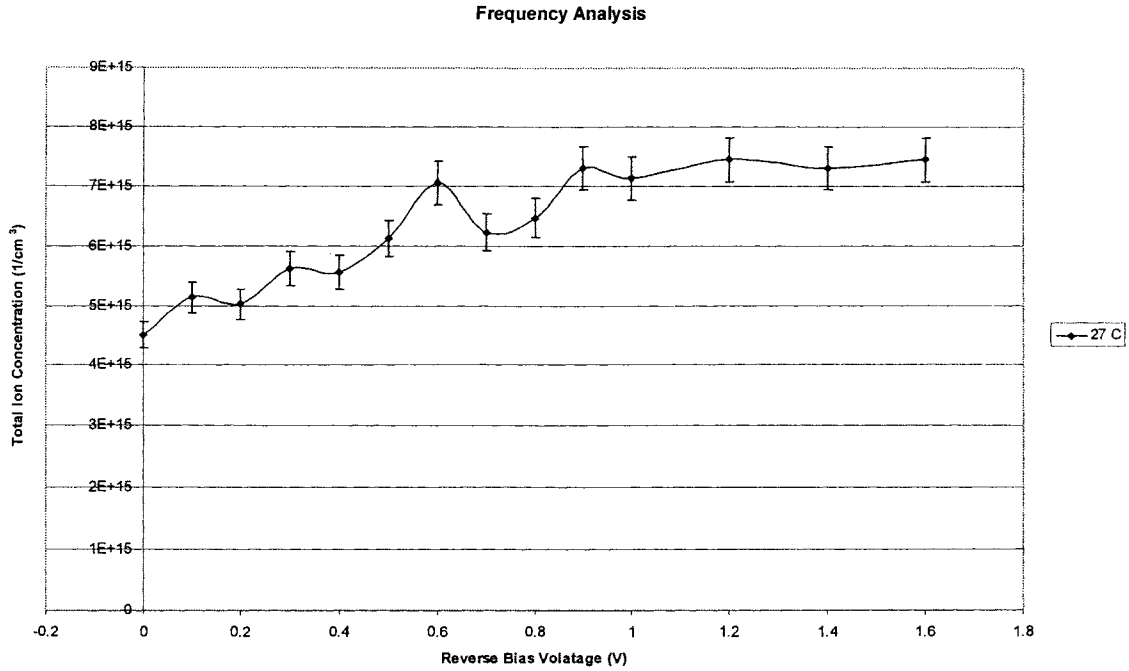

Figure 4.18. The total ion concentration for the μc-Si:H sample (2/6489) is shown as a function of reverse bias voltage for the drive frequency of 10 kHz.

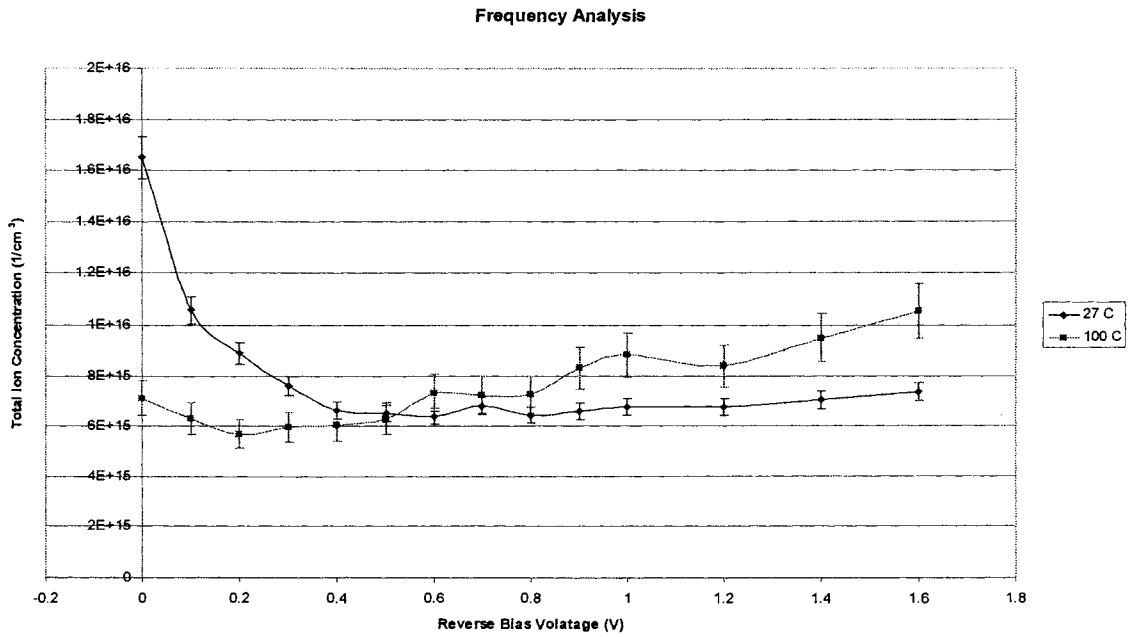

Figure 4.19. The total ion concentration for the μc-Si:H sample (2/6489) as a function of reverse bias voltage for the drive frequency of 10 kHz shows surface states at low reverse bias voltages for low and high temperatures.

The data shows by increasing temperature the defect density increases. An increase of 70 degrees uncovers addition states of $\sim 1 \cdot 10^{15}$ *1/cm*^{3}. Thus electrons are thermally stimulated into the conduction band. This is evidence of donor trap levels. The frequency dependence of the density function is shown in figure 4.20. Unexpectedly, the frequency data indicates a majority presence of acceptor traps due to the decreasing density with decreasing drive frequency. Decreasing the drive frequency from 10 kHz to 1 kHz uncovers addition trap density of $0.47 \cdot 10^{15} \pm 0.024 \cdot 10^{15}$ *1/cm*^{3}. Similarly, decreasing the drive frequency from 1 kHz to 100 Hz reveals another $0.29 \pm 0.015 \cdot 10^{15}$ *1/cm*^{3}. However, the dominating term in determining the density is temperature (see section 2.2.2.2 for the thermal emission coefficient's dependence on temperature and drive frequency), so this sample must contain both donor and acceptor traps in which the donor traps dominate.

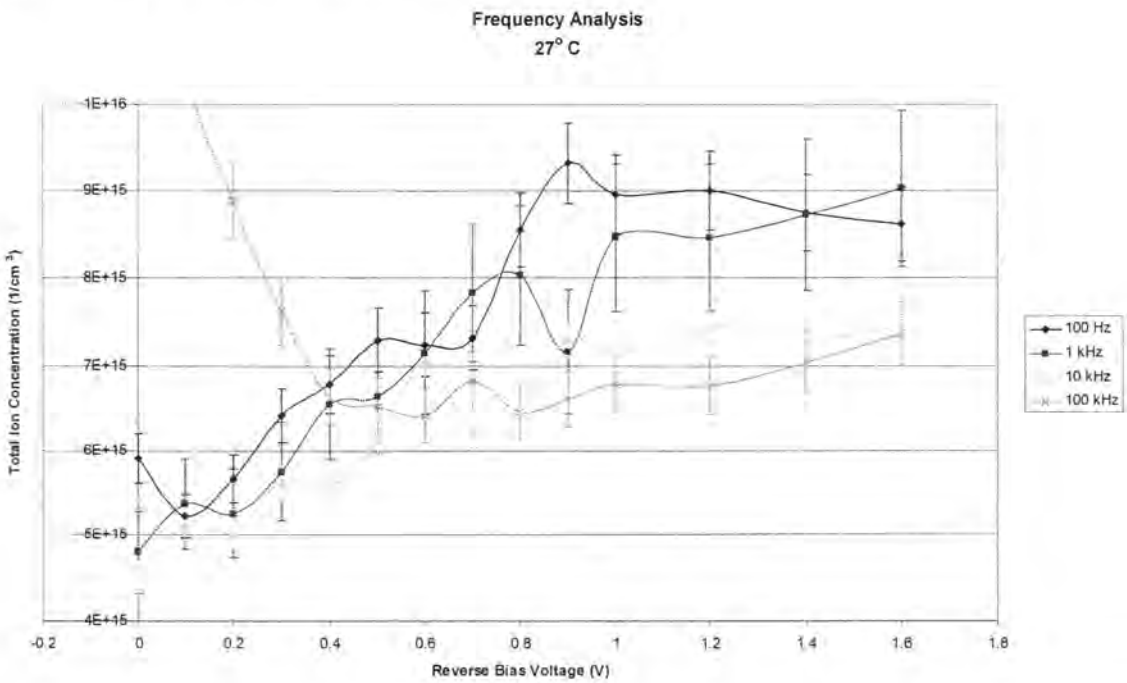

Figure 4.20. The total ion concentration for the μc-Si:H sample (2/6489) as a function of reverse bias voltage multiple drive frequencies show the frequency dependence of Kimerling's method.

Interface states are noted for the 100 kHz measurements. This may seem surprising because one would expect the surface states to behave in the same manner, but the answer lies in the nature of the material. The relatively low defect concentration within the sample suggests good passivation of the amorphous tissue. In addition, the nature of microcrystalline material proves to be a better transport than amorphous materials. Therefore, lower frequencies detect these surface states as well.

CHAPTER 5: CONCLUSIONS

5.1 a-Ge:H

Simple C-V analysis of the amorphous germanium sample shows it to have a constant background concentration of $7.55 \cdot 10^{16} \pm 0.38 \cdot 10^{16}$ $1/cm^3$ and a built-in voltage of 0.238 ± 0.022 V.

The method described by Roberts and Crowell yields no evidence of discrete traps as well as the method outlined by Cohen, et al. The latter of the two methods does however show donor trap levels and surface states. Further analysis of the sample by varying the drive frequency confirms the uniformity of the background concentration as expected.

The technique outlined by Glade, et al., estimates the trap level to be $5.6 \cdot 10^{17} \pm 0.53 \cdot 10^{17}$ $1/cm^3$ which seems very high. Again, that method is an estimate and unique to that article only in literature. This method is sensitive to variations in drive frequency and extremely sensitive to changes in temperature. This method is not desired for measuring the defect density within this sample.

Kimerling's method is a better measure of the trap concentration. This approach produces more exciting results. It shows, in agreement with theory, the existence of acceptor trap levels with a concentration of $3.32 \cdot 10^{16} \pm 0.17 \cdot 10^{16}$ $1/cm^3$. In addition, by varying both temperature and frequency, it confirms the existence of acceptor trap levels. Furthermore, it shows the existence of surface states. Kimerling's approach produces results that agree with previous measurements of the same material and SCLC measurements.

5.2 μc-Si:H

C-V measurements of the sample determined the background doping to be $4.82 \cdot 10^{15} \pm 0.0735 \cdot 10^{15}$ $1/cm^3$. The built-in voltage is found to be 0.68 ± 0.034 V.

Roberts and Crowell's approach uncovers no discrete trap levels. The method used by Cohen, et al., agrees with that conclusion. However, this method also shows the background doping to have a slight non-uniformity.

The technique by Glade, et al., is inconclusive.

Kimerling's method, although no discrete trap levels are observed, uncovers defect densities of $14.10 \cdot 10^{15} \pm 0.21 \cdot 10^{15}$ *1*/cm3 which proves the excellent hydrogen passivation of the sample. The frequency data suggested the presence of acceptor trap levels. The temperature data, which is the dominating term, shows donor traps. Therefore it is concluded that this sample consists of multiple trap types dominated by donor trap levels. Again surface states are again noted for the sample.

Although nothing significant is discovered about the microcrystalline-silicon sample, the C-V measurements do show the good passivation through use of hydrogen.

REFERENCES

[1] Ben G. Streetman, Sanjay Banerjee, Solid State Electronic Devices, Prentice Hall, 2000, 205

[2] Yuan Taur, Tak H. Ning, Fundamentals of Modern VLSI Devices, Cambridge University Press, 1998, 32

[3] G. I. Roberts, C. R. Crowell, Capacitance Energy Level Spectroscopy of Deep-Lying Semiconductor Impurities Using Schottky Barriers, *Journal of Applied Physics*, 1970, **41**, 1767-1776

[4] David V. Lang, et al., Measurement of the Density of Gap States in Hydrogenated Amorphous Silicon by Space Charge Spectroscopy, *Physical Review B*, 1982, **8**, 5285

[5] Arun Madan, Melvin P. Shaw, The Physics and Applications of Amorphous Semiconductors, Academic Press, Inc., 1988, 203

[6] E. Borchi, et al., Temperature and Frequency Dependence of the Capacitance of Heavily Irradiated Silicon Diodes, *Solid-State Electronics*, 1998, **42**, 2095

[7] G. Vincent, et al., Conductance and Capacitance Studies in GaP Schottky Barriers, *Journal of Applied Physics*, 1975, **46**, 5174

[8] M. Rösch, et al., Capacitance Spectroscopy of Defects in a-Si:H/c-Si Heterostructures, *Materials Research Society Symposium Proceedings*, 1999, **557**, 464

[9] A. Glade, et al., Frequency and Temperature Dependence of the Space Charge Capacitance in a-Si:H Films, *Journal of Non-Crystalline Solids*, 1983, **59 & 60**, 269

[10] L. C. Kimerling, Influence of Deep Traps on the Measurement of Free-Carrier Distributions in Semiconductors by Junction Capacitance Techniques, *Journal of Applied Physics*, 1974, **45**, 1839-1845

[11] John D. Jackson, Classical Electrodynamics, John Wiley & Sons, Inc, 1999, 31

[12] M. Bleicher, E. Lange, Schottky-Barrier Capacitance Measurements for Deep Level Impurity Determination, *Solid-State Electronics*, 1973, **16**, 375-380

[13] M. Sakhaf, M. Schmeits, Capacitance and Conductance of Semiconductor Heterojunctions with Continuous Energy Distribution of Interface States, *Journal of Applied Physics*, 1996, **80**, 6839-6848

[14] E. P. EerNisse, Accurate Capacitance Calculations for *PN* Junctions Containing Traps, *Applied Physics Letters*, 1971, **18**, 183-186

[15] Vikram L. Dalal, et al., Growth of High Quality a-Ge:H Solar Cells, ICAMS Conf. (2003) To be published

[16] Vikram L. Dalal, Jianhua Zhu, Joshua Koch and Joshua Graves, Electronic Transport in Microcrystalline Si:H and (Si,Ge):H, ICAMS Conf. (2003) To be published

ACKNOWLEDGEMENTS

I would like to take this opportunity to thank those people that have played a major role in helping me accomplish my research and finish up my degree at Iowa State University. First and foremost, I would like to thank my major professor, Dr. Vikram Dalal, for the opportunity and funding to research this area. Second, I would like to thank the members of my committee, also former instructors of mine, Dr. Gary Tuttle and Dr. Joseph Shinar.

I also would like to thank Max Noack for his assistance with the equipment setup and maintenance.

A special thanks goes out to the members of the Iowa State University Cyclone Football "Varsity" Marching Band (ISUCF"V"MB) for their friendship and support throughout my years at Iowa State. In addition, I would like to thank Mr. Martin Province for identifying and development of my leadership skills by appointing me to the Drum Major position for two years. A thank you also goes out to fellow Drum Majors Grif Sims, Christopher "Chip" Andringa, Jonathan DeJong, Jeff Hines and John Kauffman. Thanks to all of my dear friends in band for motivating me to finish my degree at ISU.

Finally, I would like to thank my family which played a very supportive role.

I am privileged to have all of the people mentioned play a part in my time at Iowa State and I sincerely thank all of you for all you have done for me.